Quaternary Geochronology 5 (2010) 667–678

Contents lists available at ScienceDirect

Quaternary Geochronology

journal homepage: www.elsevier.com/locate/quageo

Research Paper

Optical dating of tidal sediments: Potentials and limits inferred from the North Sea coast

B. Mauz [a,*], C. Baeteman [b], F. Bungenstock [c], A.J. Plater [a]

[a] Department of Geography, University of Liverpool, Liverpool L69 7ZT, UK
[b] Geological Survey of Belgium, Jennerstraat 13, 1000 Brussels, Belgium
[c] Lower Saxony Institute for historical coastal research, Viktoriastr. 26/28, D-26382 Wilhelmshaven, Germany

ARTICLE INFO

Article history:
Received 21 August 2009
Received in revised form
20 May 2010
Accepted 21 May 2010
Available online 1 June 2010

Keywords:
Optical dating
Tidal sediments
North Sea

ABSTRACT

The accuracy of optical ages derived from tidal sediments depends largely upon the transport processes. These processes constrain the degree of bleaching by the time of deposition and the choice of grain size for dating. This study looks at flow regime, sediment bedding, particle size and suspended sediment concentration (SSC) over tidal flats in order to identify the tidal sub-environment from which reliable multigrain optical ages are most likely to be achieved. The resulting conceptual model is then compared with empirical OSL data obtained from Holocene sediments of the southern North Sea tidal coastal plain of continental Europe. Optical dating of the tidal sediments included single-aliquot-regenerative dose protocol applied to multigrain aliquots of fine sand and fine silt, statistical analysis using weighted skewness, standardised kurtosis and over-dispersion. It is inferred from the model that smaller grains should be better bleached than larger grains. However, because transport and deposition processes are extremely variable in both space and time, unequivocal "bleaching rules" could not be assigned to a particular tidal sub-environment. In this context more than 85% of our samples return accurate ages and around 13% of our optical ages are overestimated when compared with ages from established well-constrained stratigraphic frameworks. The empirical study confirms the concept of "variable bleaching rules": both accurate and inaccurate ages are obtained from silty and sandy OSL samples regardless of the sub-environment and well-bleached samples may be obtained from all tidal sub-environments. Although our study is based on multiple-grain aliquots it also shows that an independent statistical treatment of equivalent dose data is an indispensable procedure to detect and correct for insufficient bleaching.

1. Introduction

Optical dating is an alternative to radiocarbon dating for sediments lacking appropriate organic material for radiocarbon dating. With tidal sediments the technique is of particular interest as organic material is barely available or of uncertain relation to the depositional event, thus yielding inaccurate or erroneous ages (e.g. Baeteman, 2008). Dating Holocene coastal marine sediments is required for any sea-level study or palaeoenvironmental reconstruction that, for example, aims to determine the response of coast to sea-level trends in order to assess the future sensitivity to and impacts of sea-level rise. Hence, there is considerable scope for a more detailed study on the performance of the optical dating technique on tidal sediments and the reliability of optical ages for palaeoenvironmental reconstruction.

In a tidal environment the accuracy of the optical ages depends upon the processes of transport and deposition, sediment composition, sedimentation rate, the nature of wetting and drying, and post-depositional radionuclide mobility. The specific challenge for OSL dating is derived from the degree of bleaching at time of deposition and from availability of the dosimeter in the appropriate grain size. We address here the depositional processes on a tidal flat with regard to flow regime, sediment bedding, particle size and suspended sediment concentration (SSC) in order to establish a generic sedimentary sub-environment where sufficient bleaching is most likely and, hence, dating more likely to be successful. The resulting conceptual model is compared with published (Mauz and Bungenstock, 2007) and new OSL data from Holocene sediments obtained from the southern North Sea coast (French, Belgian and German coasts).

* Corresponding author.
E-mail address: mauz@liv.ac.uk (B. Mauz).

1871-1014/$ – see front matter © 2010 Elsevier B.V. All rights reserved.
doi:10.1016/j.quageo.2010.05.004

For the Belgian coastal plain an exceptional sedimentary data set from closely-spaced boreholes is available, enabling reconstruction of its Holocene evolution in great detail in both time and space (Baeteman and Declercq, 2002; Baeteman, 2008). The accuracy of the OSL ages may then be assessed by comparing the OSL ages resulting from an independent statistical protocol (Bailey and Arnold, 2006; Arnold and Roberts, 2009) with the expected ages. We focus exclusively on the bleaching of Holocene tidal sediments for OSL dating and do not touch upon general OSL dating issues (e.g. saturation and other properties of the dosimeter).

2. Previous studies

Plater and Poolton (1992) studied fine-silt feldspars using infrared stimulated luminescence (IRSL, 940 nm) and thermoluminescence (TL). The samples were extracted from a sediment core that showed a change in environment from the high-water mark to the low-water mark of the mudflat and a short-lived reversal to more marine condition probably caused by a storm surge. For IRSL the authors find well-bleached feldspars in the upper and lower part of the mudflat while the residual TL progressively increases with decreasing daylight exposure time during the intertidal period linked to altitude on the tidal flat. Clarke and Rendell (2000) examined the fundamental characteristics of IRSL in intertidal sediments, and Bailiff and Tooley (2000) dated alternating marine and freshwater sediments using silt-sized feldspars. With an average uncertainty of around 14% the IRSL ages are generally consistent with radiocarbon ages derived from intercalated peat. Bailiff and Tooley's study highlights important issues arising from intertidal sediments such as changing water content and the presence of unsupported uranium alongside organic sediment components. Richardson (2001) undertook a comprehensive study on bleaching in tidal environments showing that feldspars deposited in intertidal mud and in saltmarsh are not bleached on a multiple grain aliquot level. Hong et al. (2003) studied a sandy tidal flat at the southwest coast of the Korean peninsula and find well-bleached K-rich feldspars and stratigraphically consistent IRSL ages between ~40 a and 120 a. Madsen et al. (2005) studied a tidal mudflat in the northern part of the Danish Wadden Sea and compared the optical ages with ^{210}Pb and ^{137}Cs data. These authors tested the reliability of quartz optical ages, finding well-bleached fine sand quartz grains (90–180 μm) in the mudflat and optical ages spanning ~7–315 a, which are in agreement with the independent age control. This study made detailed considerations on the environmental radioactivity in relation to water and organic matter content. The calculation of the environmental dose rate accounted for excess ^{210}Pb and changing beta and gamma dose to which quartz grains are exposed in a constantly accreting sediment setting. Boomer and Horton (2006) used IRSL ages derived from lower to upper intertidal mudflats to reconstruct sea-level index points. All ages presented in this study are in stratigraphic order and in accordance with the radiocarbon ages of the underlying peat. Roberts and Plater (2005, 2007) dated Holocene tidal flat and subtidal shoreface deposits (125–150 μm and 150–180 μm quartz grains). Samples appeared to be effectively and consistently zeroed, giving a series of well-constrained ages over the period of ~4700–440 years ago, correctly ordered according to stratigraphy and sedimentary geometry. Tidal flat sediments collected from the present-day shoreline returned zero ages within analytical uncertainty (Roberts and Plater, 2005). Madsen et al. (2007a, b) dated fine sand quartz grains (90–180 μm and 180–250 μm) extracted from sediment cores retrieved from salt marshes of the Danish Wadden Sea. The resulting ages enabled the calculation of sedimentation rates which were consistent with the geological estimate. While all these studies used fine sand grains, Mauz and Bungenstock (2007) dated fine-silt quartz grains extracted from mudflat sediments at the German North Sea coast. All but two OSL ages fell into the expected time interval but no independent age control was available for individual samples.

For further information, Jacobs (2008) reviews luminescence dating development and application for coastal and marine sediments.

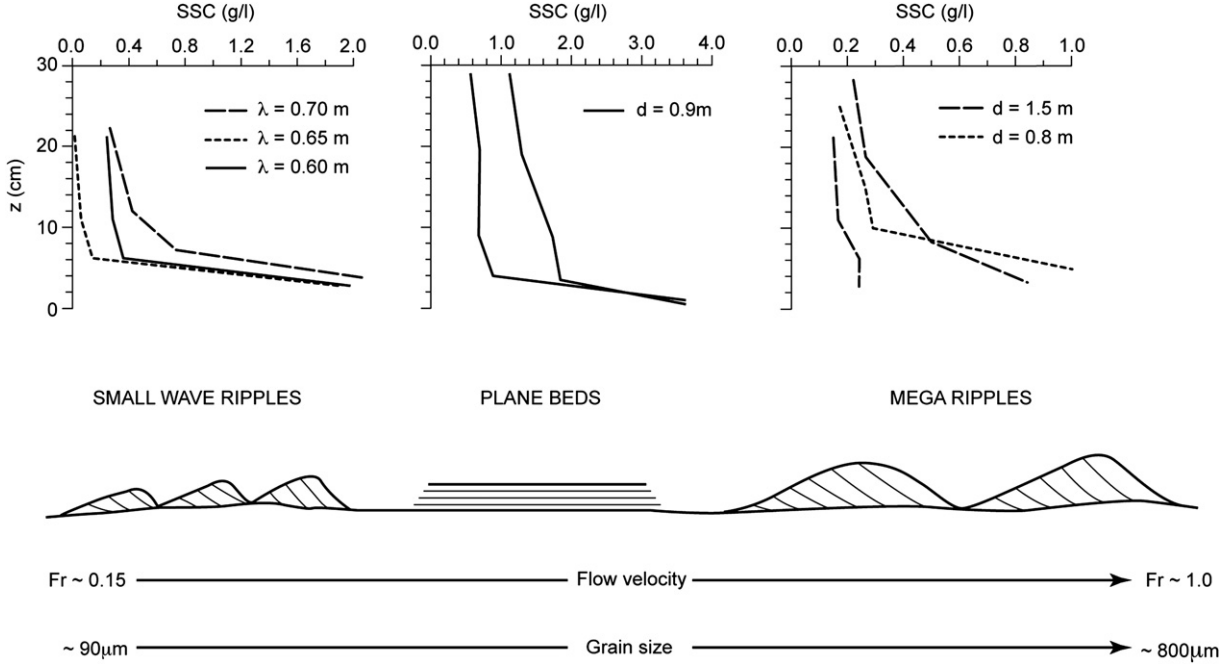

Fig. 1. Simplified illustration of the relationship between flow regime (Froude number, Fr), sediment bed, grain size and suspended sediment concentration (SSC). SSC data are from the SE Australian coast (Nielsen, 1984). Note that this illustration does not account for the lateral change of setting due to e.g. bidirectional flows. λ = wavelength; d = water depth.

Table 1
Conceptual frame of tidal and wave processes and the link to daylight exposure of sediments grains during tidal cycle.

Tidal cycle period and process	Tide	Wave	Bleaching
Ebb tide, exposure of intertidal flat	N/A	N/A	Unrestricted, with the exception of pools; limited to surface few mm, bleaching depth dependent upon grain size and algae colonies
Early flood tide, sediment reworking by waves in advancing surf zone	Negligible-waxing	Significant wave action causing sediment re-suspension. High-frequency fluctuation in turbidity (higher during breaking, lower during shoaling and post-breaking)	Effectiveness determined by location relative to wave break-point – higher efficiency in swash zone, lower in surf zone, lowest in zone of wave shoaling
Flood tide, sediment transport within water column and along bed	Significant tidal currents orientated onshore (generally fastest at mid-tide). Finer sediments carried in suspension and intermittent suspension, coarser fraction transported as traction load.	Negligible	Effectiveness decreasing with increasing water depth, determined by SSC. Bleaching efficiency significantly limited for traction load
Late flood tide/slack water, particle settling linked to grain size and flocculation	Waning-negligible	Some wave action in shallow water (water depth < wave base)	Effectiveness determined by water depth (i.e. location/altitude on the tidal flat relative to high water) and residual turbidity. Bleaching likely to be more effective for fines retained in water column
Ebb tide, potential for sediment re-suspension and reworking	Waxing-significant tidal currents orientated offshore. Extent of ebb-current reworking linked to location/altitude on the tidal flat – limited on upper part, improved on lower part where ebb currents have sufficient time to gather speed and entrain sediment. Finer sediments carried in suspension and intermittent suspension, coarser fraction transported as traction load.	Negligible	Effectiveness decreasing with increasing water depth, determined by SSC. Bleaching efficiency significantly limited for traction load
Ebb tide, shallow-water wave reworking as ebb tide shoreline leaves the tidal flat	Negligible	Significant wave action causing sediment re-suspension. High-frequency fluctuation in turbidity (higher during breaking, lower during shoaling and post-breaking)	Effectiveness determined by location relative to wave break-point – higher efficiency in swash zone, lower in surf zone, lowest in zone of wave shoaling
Ebb tide, exposure of intertidal flat	N/A	N/A	Unrestricted, with the exception of pools; limited to surface few mm, bleaching depth dependent upon grain size and algae colonies; effectiveness dependent upon sedimentation rate

3. OSL dating of tidal sediments

3.1. Bleaching in tidal environments

Tidal flats are characterised by a shore-normal energy gradient which is the result of increasingly higher relative elevation of the flat landward of the sea and of tidal channels. The most important consequences of this energy gradient are shore-normal grain size sorting, reduction of water depth and reduction in the frequency and duration of tidal inundation. The mechanism of sediment transport over the flat is driven by cyclical tidal currents and shallow-water waves, which drive the flow regime over the flat. The typical flow velocity over a tidal flat (0.3–3 m s^{-1}, e.g. Andersen and Pejrup, 2001) creates subcritical laminar (Froude number Fr <1) to supercritical turbulent (Fr >1) flows, all capable of entraining sand-sized particles (Fig. 1; Miller et al., 1977) which is the size most commonly used in optical dating (i.e. <300 μm).

In general, sand-sized grains move by rolling, sliding and saltation (intermittent suspension), whilst finer grain sizes are transported in suspension. The highest suspended sediment concentration (SSC) occurs relatively close to the sediment–water interface (e.g. 2 g l^{-1}, Nielsen, 1984; Fig. 1). Sand-sized grains are in suspension during several tidal cycles, but the suspended sediment layer is probably only a few cm above the sediment–water interface (Fig. 1).

Intertidal exposure provides a further opportunity for bleaching, but only the surface layer of grains is exposed to daylight. The efficiency of this bleaching mechanism for the incremental accumulation of sediment on each tidal cycle will be highly dependent upon sedimentation rate. Furthermore, the duration of this exposure will be the inverse of inundation period. On mudflats the average water depth is lower and the period of subaerial exposure per tidal cycle is longer than on sandflats. However, the SSC is generally higher on mudflats than on sandflats because reworking of sediments is inversely correlated with water depth (Pejrub, 1986). The SSC increase is spatially variable depending upon estuarine mixing, location of the resulting maximum SSC (turbidity maximum), and the relative balance between marine and terrestrial sediment influx. The turbidity maximum is usually situated landward of the salt-water injection point where salinity is low (10–15‰). At the turbidity maximum, flocculation may occur causing rapid settling of particles and extreme SSC values at the water–sediment interface of up to 100 g l^{-1}. In our study area SSC varies between 0.1 g l^{-1} and ~1.0 g l^{-1} (e.g. Merckelbach and Ridderinkhof, 2006).

From previous studies that measured TL and IRSL of feldspar silt-sized grains it has to be inferred that suspended sediment concentration reduces the efficiency of bleaching of grains within and beneath the water column (Berger, 1990; Ditlefsen, 1992). The maximum SSC under which sand- and silt-sized quartz and

feldspar grains are sufficiently bleached is, however, essentially unknown. The only study that quantifies SSC alongside the degree of bleaching is from Ditlefsen (1992). He measured the IRSL signal of 100–200 μm K-rich feldspars and found a substantial reduction of bleaching under 0.01 g l^{-1} SSC. Under 0.05 g l^{-1} SSC feldspar grains were virtually unbleached after 20 h exposure to light. But the results of Ditlefsen (1992) and Berger (1990) are not directly comparable to our approach because both studies did not measure the quartz 'fast' luminescent component of the suspended grains. Richardson (2001) and Sanderson et al. (2007) give useful additional information: in an estuarine environment light levels are reduced by three orders of magnitude in the upper 80 cm of the water column (Richardson, 2001) and wavelengths shorter than 500 nm and longer than 750 nm are reduced to a negligible level at 1.5 m water depth (Sanderson et al., 2007).

From the perspective of sediment recycling over longer timescales, it is important to consider the reworking processes of tidal deposits. Recycling occurs alongside re-suspension of grains, and this process is only useful for bleaching if it results in the breakdown of bonds between organic aggregates and pellets to allow individual grains to flow freely. The breakdown is controlled by chemical (total alkali in the sediment), biological (algal mats) and energetic (>0.3 m s^{-1} for silty quartz: Hjulstrøm, 1935) conditions. Sand suspension on the other hand is less dependent upon water chemistry and requires less water energy (<0.3 m s^{-1}: Hjulstrøm, 1935). Madsen et al. (2007b) speculated that intertidal sediments are effectively zeroed because tidal currents and wave action cause considerable re-suspension and reworking of surface sediments. Andersen et al. (2006) quantified reworking at the North Frisian coast and found bed-level changes triggered by seasonal changes of the tidal regime which were one to two orders of magnitude greater than the annual sediment accretion rate. Similarly, some degree of sediment recycling across the surface was observed between mudflat and tidal channel as a function of storm versus fair-weather conditions (Andersen et al., 2006). Significant sediment recycling takes place through lateral migration of tidal channels and creeks (e.g. Reineck, 1958 for the East Frisian coast) but occurs alongside high SSCs. Thus, it must be the frequency of sediment re-suspension during the reworking process that induces sufficient bleaching. This frequency depends upon tidal asymmetry, frequency of onshore storms and type of tidal regime (e.g. semi-diurnal).

When accommodation space exceeded sediment supply, e.g. during early Holocene rapid sea-level rise, numerous, less mobile tidal inlets and channels dominated the coastal plain (e.g. van der Spek and Beets, 1992 for the mesotidal Holland tidal basin). With the mid-Holocene reduction of sea-level rise tidal flats expanded, migration rate of tidal channels increased and hence, the extent of sediment reworking increased. Thus, sediment recycling over the longer term is more likely to occur under scenarios of reduced sea-level rise or increased sediment supply, providing that the tidal flats do not convert to extensive emergent salt marshes.

Table 1 shows that, when combined, the influences of transport and deposition processes, the interaction of tide- and wave-induced sediment transport, and the efficacy of subaerial exposure during low-water ebb tide dictate a high level of spatial and temporal variability in the degree of bleaching that makes it difficult to generalize on the bleaching efficiency according to tidal sub-environment.

3.2. Environmental dose rate in tidal environments

Tidal sediments on the North Sea coast are characterised by a high degree of sorting, homogeneous composition, various amount of organic matter and relatively high sedimentation rate,

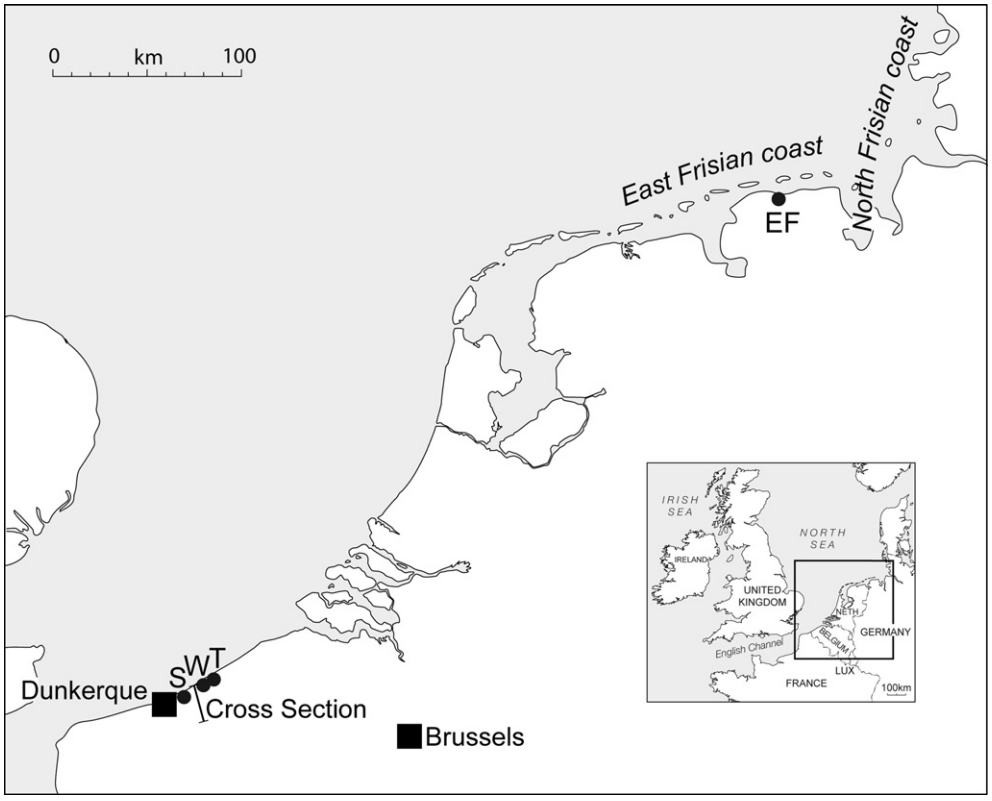

Fig. 2. Map of the southern North Sea coast showing origin of samples studied here. T = Toevlucht site, W = Wulpen site, S = French site, EF = East Frisian site; black bar: location of cross section displayed in Fig. 3.

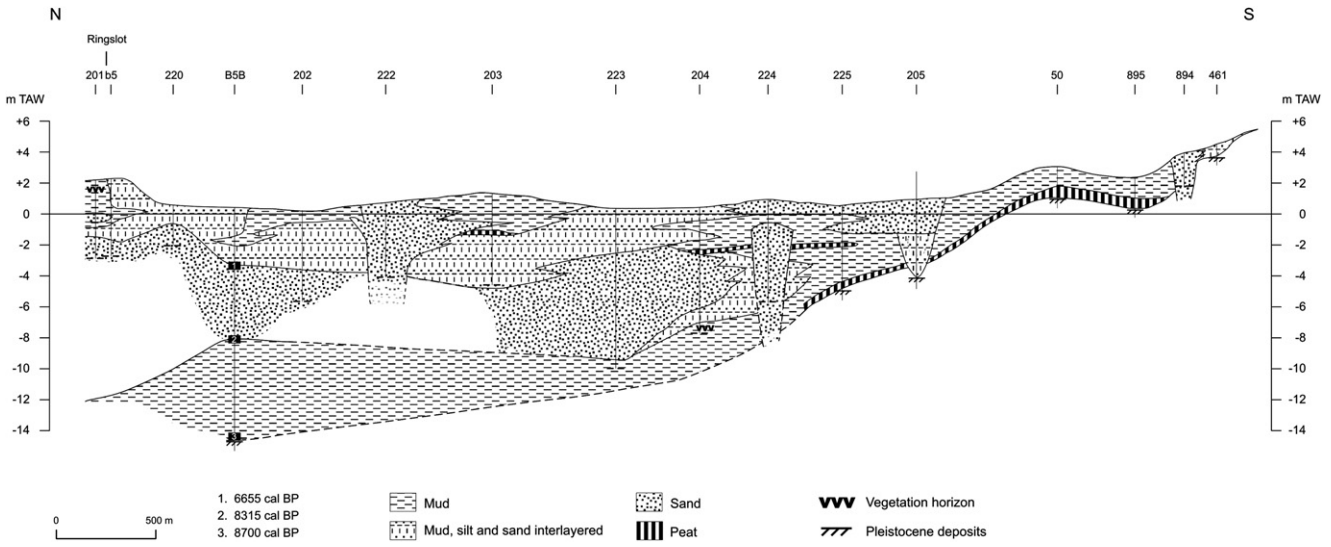

Fig. 3. Cross section of the Belgian-French coastal plain illustrating the Holocene sedimentary succession.

particularly in tidal channels. In such an environment the matrix is heterogeneous for beta radiations due to non-uniform distribution of potassium-rich feldspars which are the dominant beta-emitters. For beta radiations of these emitters the infinite matrix (Aitken, 1985) is reached after around one year. For gamma radiations the infinite matrix is reached after 30 years and matrix inhomogeneity is insignificant.

A significant uncertainty of the dose rate estimate is derived from the daily, fortnightly, monthly and annual change of water level and the oscillating pore water associated with it. Bailiff and Tooley (2000) simply estimated it to 5%. Roberts and Plater (2005) compiled a water content model based on particle size distribution and pore space saturation during intertidal exposure. Hence, sites on the upper part of the intertidal flat drain freely for some part of the ebb period, whilst those on the shoreface remain saturated for 100% of the time. This water content history for a tidal cycle could be estimated for the long term on an iterative basis with reference to known trends in relative sea level during the period since deposition.

4. Study sites and age constraints

At the Belgian coastal plain data from about 1150 undisturbed hand-augered gouge cores at a separation of 50–350 m are available. Also, data from 100 undisturbed mechanically-drilled cores are available; 50 of these cores were drilled in sand-filled tidal channels and two of these are studied here. These cores recover the entire Quaternary sequence. Over 200 radiocarbon dates obtained

Table 2
The samples investigated in this study: origin, depositional environment and age constraint. Water depth of tidal channels is given with respect to mean low water.

Sample code	Origin	Sediment	Tidal sub-environment	Age constraint (ka)
LV35	French coast	Massive sand	Sandflat (intertidal)	2.0 ± 0.5
LV40	French coast	Massive sand with shell debris, lenses of peat detritus and mud drapes	Tidal channel (subtidal, 2–7 m water depth)	4.5 ± 0.8
LV41	French coast	Massive sand with shell debris, thinly interlayered silt and peat detritus	Tidal channel (subtidal, 2–7 m water depth)	6.0 ± 0.8
LV42	French coast	Massive sand with shell debris	Tidal channel subtidal, water depth 2–7 m)	4.0 ± 0.8
LV43	French coast	Massive sand with mud drapes and shell debris	Tidal channel (subtidal, 1–6 m water depth)	5.0 ± 0.8
LV44	French coast	Massive fine sand	Sandflat (intertidal)	4.5 ± 0.8
LV45	French coast	Massive sand with shell debris	Tidal channel (subtidal, water depth 1–5 m)	3.5 ± 0.5
LV47	French coast	Massive sand	Tidal channel (subtidal, water depth 2–7 m)	3.0 ± 0.8
LV48	French coast	Massive sand with root penetrations	Tidal channel (subtidal, 1–6 m water depth)	>5
LV226	Belgian coast (Toevlucht)	Massive fine sand with few clay lenses	Tidal channel (subtidal, 1–5 m water depth)	<2.3
LV227	Belgian coast (Toevlucht)	Massive fine sand with few clay flasers and clay pebbles	Tidal channel (subtidal, 1–5 m water depth)	<2.3
LV228	Belgian coast (Toevlucht)	Erosive lag: fine sand with shell debris and few clay lenses	Tidal channel (subtidal, 5–10 m water depth)	<3
LV345	Belgian coast (Toevlucht)	Bioturbated silty clay	Mixed flat (intertidal)	0.9 ± 0.1
LV231	Belgian coast (Wulpen)	Thinly laminated silt/sand with few clay lenses	Tidal channel (subtidal, 1–6 m water depth)	<2.3
LV232	Belgian coast (Wulpen)	Massive fine sand with thin clay lenses and small clay pebbles	Tidal channel (subtidal, 5–10 m water depth)	1.3 ± 0.8
LV233	Belgian coast (Wulpen)	Massive fine silty sand with thin wavy clay laminae	Tidal channel (subtidal, 1–5 m water depth)	6.3 ± 1.2
LV01	East Frisian coast	Plane parallel laminated mud	Mudflat	1.2 ± 0.8
LV02	East Frisian coast	Massive mud	Mudflat	1.2 ± 0.8
LV03	East Frisian coast	Massive mud	Mudflat	1.2 ± 0.8
LV04	East Frisian coast	Massive mud	Mudflat	1.2 ± 0.8
LV06	East Frisian coast	Mud with thin layers of fine sand	Mudflat	1.2 ± 0.8
LV08	East Frisian coast	Mud with thin layers of fine sand	Mudflat	1.2 ± 0.8
LV09	East Frisian coast	Plane parallel laminated mud	Mudflat	1.2 ± 0.8
LV10	East Frisian coast	Massive mud	Mudflat	1.2 ± 0.8

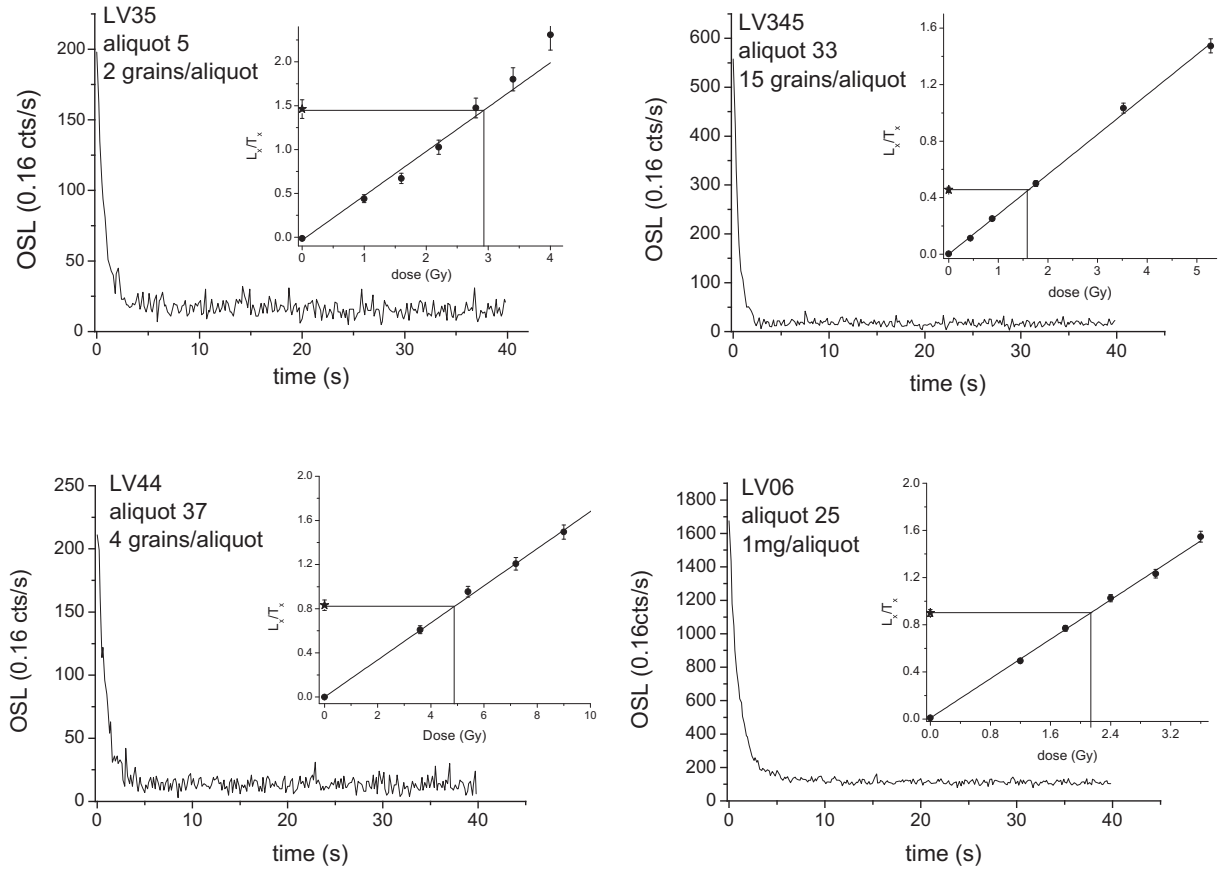

Fig. 4. OSL decay curves and dose response curves. Examples from samples measured with different numbers of luminescent grains per aliquot.

from top and base of peat beds and from shells provide the chronology through the entire Holocene sequence (Baeteman and Declercq, 2002). The detailed stratigraphy of the sedimentary succession was established by means of cross-sections where the boreholes have been correlated on the basis of facies of sedimentary environments (e.g. Fig. 3). The sedimentological characteristics of the late-Holocene deposits have been investigated in numerous shallow outcrops that were temporarily accessible together with radiocarbon dates (Baeteman, 2005, 2008) obtained from intertidal mollusc shells. The intensive geological investigations provided the data to establish the sea-level reconstruction (Denys and Baeteman, 1995), the history of the sedimentary infill of the area (Baeteman et al., 1999), the driving mechanisms of coastal changes (Baeteman, 2005, 2008; Baeteman et al., 1999, 2002), and a reconstruction of the palaeogeography at different time slices since 9500 cal BP (Baeteman and Declercq, 2002). Age constraints by which the accuracy of the OSL ages was evaluated were achieved by linking the dated sediment samples to the palaeogeographic framework for the Belgian coastal plain (Baeteman and Declercq, 2002). This approach was also adopted to the tidal flat system located around 25 km further south on the French coastal plain (Fig. 3).

Similarly to the Belgian coast, a detailed stratigraphy of the sedimentary succession was established for the East Frisian coastal plain through borehole data and sediment facies correlation (e.g. Streif, 2004) allowing for reconstructing the regional sea-level history (Bungenstock and Schäfer, 2009). The basin-wide Upper Peat (3500–2200 cal BP) provides the termine post quem for the sedimentary infill of the tidal basin. A second peat, recorded only in places, provides a time marker for 2000–1500 cal BP (Streif, 2004). Our OSL samples are derived from sediments overlying this marker. They must therefore be younger than 1750 ± 250 a and older than 500 a when large-scale embankment (Van Lengen, 1978) prevented tidal inundation of the study site.

Sampling for radiocarbon and optical dating is governed by the availability of the appropriate material and therefore, the quality of the age constraint depends upon the degree of spatial and temporal resolution of the palaeogeographic reconstruction. The uncertainty associated with our age constraints is therefore variable depending on the vertical and lateral proximity of the OSL sample to a radiocarbon age. For the Belgian and French coastal plain the uncertainty lies between 500 a and 800 a and ~1000 a for the East Frisian coastal plain.

4.1. Samples

All samples were obtained from sediment cores retrieved from southern North Sea coastal plains. At the French coast these cores (S-cores, Fig. 2) were retrieved from boreholes drilled in the coastal plain to depths of 5–10 m and analysed by Mrani Alaoui (2006). Around 25 km further north, at the Belgian coast two c 20 m deep boreholes were drilled close to the edge of the wide sand-filled tidal inlet (Toevlucht) and in a palaeochannel of the river IJzer (Wulpen, Fig. 2) filled with tidal sand. At the East Frisian coast cores were recovered from boreholes drilled into the mudflat behind the barrier island of Langeroog (Mauz and Bungenstock, 2007; Fig. 2).

5. Methods

Samples were prepared using conventional techniques to extract fine to medium quartz grains from the sediment and

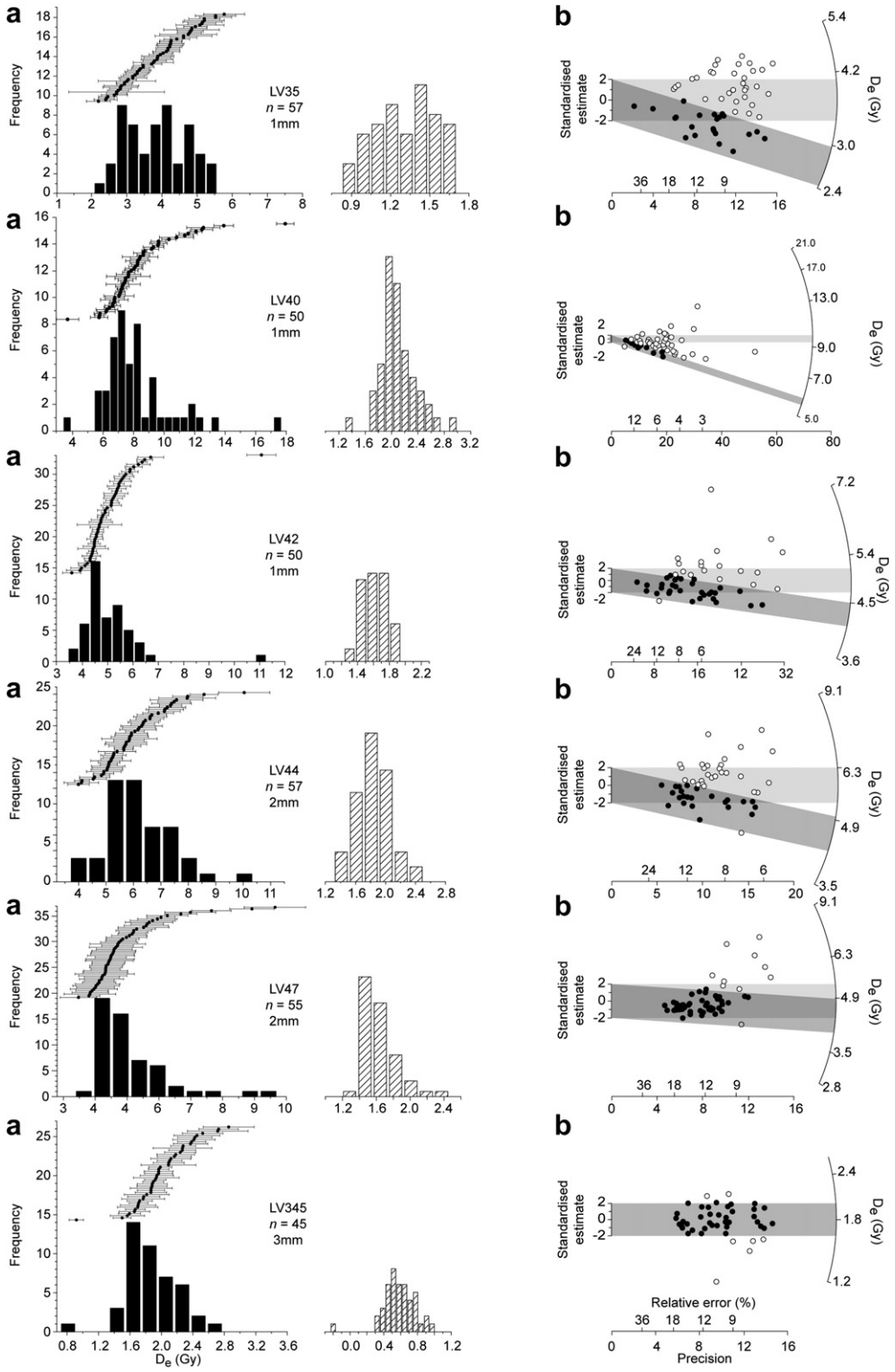

Fig. 5. Dose distribution of accepted aliquot data of representative samples studied here. a: Black bars show normal D_e values, grey bars show ln D_e values, dots with error bars show ranked D_e values. b: radial plot of the same sample. Light shaded bar points to the mean D_e estimate, dark shaded bar points to the model D_e estimate. All model D_es were derived from MAM-3 statistics.

additionally treated in 48% HF for 80 min to remove the outer part of the grain affected by alpha radiation (Mauz et al., 2002). A standard single-aliquot-regenerative dose (SAR) protocol was employed for D_e determination (Murray and Wintle, 2000) using 1–5 mm aliquots depending on the OSL sensitivity (i.e. OSL output per unit beta dose) of the sample. All samples were tested for feldspar contamination using the IR–OSL depletion ratio (Duller, 2003). The preheat was chosen on the basis of a dose recovery test. The test dose was 5–40% of the expected D_e depending on the sensitivity of the quartz sample. The integral over the first 0.8 s and

Table 3
Details of OSL statistics. Number of luminescent grains per aliquot was estimated following Duller (2008); σ = over-dispersion; c = weighted skewness of ln D_e; $1\sigma_c$ = standard error of skewness (critical skewness score: $\pm1\times\sigma_c$); k = standardised kurtosis; $1\sigma_k$ = standard error of kurtosis (critical kurtosis score: $\pm1\times\sigma_k$); MAM-3 = minimum age model with 3 parameters; CAM = central age model.

Sample code	Aliquot# (accepted/measured)	OSL grain size (μm)	Aliquot size/weight	Luminescent grains/aliquot	Descriptive statistics					Statistical age model
					σ (%)	c	$1\sigma_c$	k	$1\sigma_k$	
LV35	57/144	160–200	1 mm	2	23	−0.24	0.32	−1.01	0.64	MAM-3
LV36	47/96	90–160	1 mm	4	15	−0.08	0.36	−0.53	0.71	CAM
LV40	54/96	90–160	1 mm	4	27	0.75	0.31	16.85	0.63	MAM-3
LV41	64/96	90–160	1 mm	4	14	−0.10	0.31	0.27	0.61	CAM
LV42	50/72	90–160	1 mm	4	19	1.68	0.35	12.03	0.69	MAM-3
LV43	54/72	90–160	1 mm	4	21	0.26	0.33	0.88	0.67	MAM-3
LV44	51/168	150–200	2 mm	4	20	0.22	0.34	0.89	0.69	CAM/MAM-3
LV45	48/72	150–200	3 mm	6	16	−0.40	0.35	−0.6	0.71	CAM
LV46	68/120	90–150	2 mm	9	17	–	–	–	–	Arithm mean
LV47	55/144	150–200	2 mm	4	20	1.40	0.33	3.97	0.66	MAM-3
LV48	55/84	90–150	2 mm	9	15	–	–	–	–	Arithm mean
LV226	49/58	90–125	5 mm	20	13	–	–	–	–	Arithm mean
LV227	54/124	90–125	5 mm	20	46	–	–	–	–	Arithm mean
LV228	36/60	150–200	4 mm	14	51	–	–	–	–	Arithm mean
LV345	45/96	90–212	3 mm	15	20	–	–	–	–	Arithm mean
LV231	36/48	90–125	5 mm	20	8	–	–	–	–	Arithm mean
LV232	44/72	90–125	3 mm	12	18	–	–	–	–	Arithm mean
LV233	30/72	90–125	2 mm	12	18	–	–	–	–	Arithm mean
LV01	39/48	4–15	1 mg	–	–	–	–	–	–	Arithm mean
LV02	47/48	4–15	1 mg	–	–	–	–	–	–	Arithm mean
LV03	55/72	4–15	1 mg	–	–	–	–	–	–	Arithm mean
LV04	47/48	4–15	1 mg	–	–	–	–	–	–	Arithm mean
LV06	62/72	4–15	1 mg	–	–	–	–	–	–	Arithm mean
LV08	53/72	4–15	1 mg	–	–	–	–	–	–	Arithm mean
LV09	46/48	4–15	1 mg	–	–	–	–	–	–	Arithm mean
LV10	37/48	4–15	1 mg	–	–	–	–	–	–	Arithm mean

over the last 10 s of the OSL stimulation were used for OSL and background determination, respectively. The following criteria were applied for rejection of aliquot data for D_e determination: (i) signal to noise ratio of the test dose OSL is <12; (ii) recycling ratio is outside 1 ± 0.1; (iii) the recuperation signal is >5% of the natural signal; (iv) the relative standard error of D_e is >20% and (v) the first regenerative OSL test dose (T_{R1}) is more than 20% larger than the natural OSL test dose (T_N) indicating that a significant sensitivity change took place between the measurement of the natural and the first regenerative dose. The aliquot size was chosen to be as small as possible and was increased with decreasing OSL sensitivity of the quartz sample. The number of luminescent grains per aliquot was estimated following Duller (2008).

For samples with $n > 50$ aliquots (Rodnight, 2008) and ≤9 luminescent grains per aliquot the statistical approach followed Bailey and Arnold (2006) and Arnold and Roberts (2009) where the critical statistical variables are weighted skewness (c), standardised kurtosis (k) and over-dispersion (σ). The variables were calculated using the quadrature of errors derived from standard error of D_e and 6% over-dispersion. The 6% over-dispersion accounts for the dose heterogeneity of the samples which is presumably small due to the homogeneous composition and well sorted nature of the sediments. The decision protocol based on critical values of these variables led to the choice of the statistical model to be used for D_e estimation. The degree of over-dispersion ($20\% > \sigma > 20\%$) was used to choose between the application of the central age model (CAM, Galbraith et al., 1999) or minimum age model (MAM, Galbraith et al., 1999). The mean of the lowest 5% of D_e values (Olley et al., 1998) requires an empirical 'calibration' to a known-age sample and was therefore not adopted here. For aliquots with ≥12 luminescent grains the statistical approach followed the arithmetical mean of D_e values.

The activity of K, Th and U in the sediment was estimated using neutron activation analysis (NAA, for samples LV01-LV48) and high resolution low-level gamma spectrometry (for samples LV226-233 and LV345), converted to dose rate using conversion factors provided by Adamiec and Aitken (1998) and corrected using beta attenuation factors in grains (Brennan, 2003). The cosmic dose rate was derived from the mean burial depth of the samples (Prescott and Hutton, 1994) with a 5% uncertainty. The alpha dose of fine-silt samples was corrected for alpha efficiency using a-values between 0.03 and 0.04 determined using a modified SAR protocol (Mauz et al., 2006). The water content was estimated on the basis of the measured field moisture applying a model modified from Roberts and Plater (2005). Dose rate values derived from NAA technique were further corrected for organic matter using absorption factors reported by Lian et al. (1995).

The quality of the OSL ages was assessed using the following approach: (i) where an age constraint with a reasonable uncertainty (i.e. <800 a) is available, the accuracy of the OSL age can be assessed by comparing the difference between the ages using $\sqrt{a^2+b^2}$, where a and b are the 2σ errors of the age constraint and the OSL age respectively; (ii) where an age constraint without an uncertainty is available, the OSL age is assessed in terms of its stratigraphic consistency and is labelled correct/incorrect.

6. Results

With reference to the conceptual approach about bleaching in a tidal environment no unequivocal relationship between depositional environments, suspended sediment concentration and degree of bleaching was found.

From the 24 samples investigated 2 samples represent intertidal sandflats, 13 samples are derived from subtidal channels of various sizes and depths and 9 samples are from intertidal mudflats or mixed flats (Table 2). About 25–70% of aliquots were rejected (Table 2) following the rejection criteria (i), (ii) and (iii) which address the OSL sensitivity of the quartz. As a consequence of the low sensitivity, from 16 sand samples only 5 samples could be measured using the smallest aliquot size possible (see Fig. 4 for OSL decay and

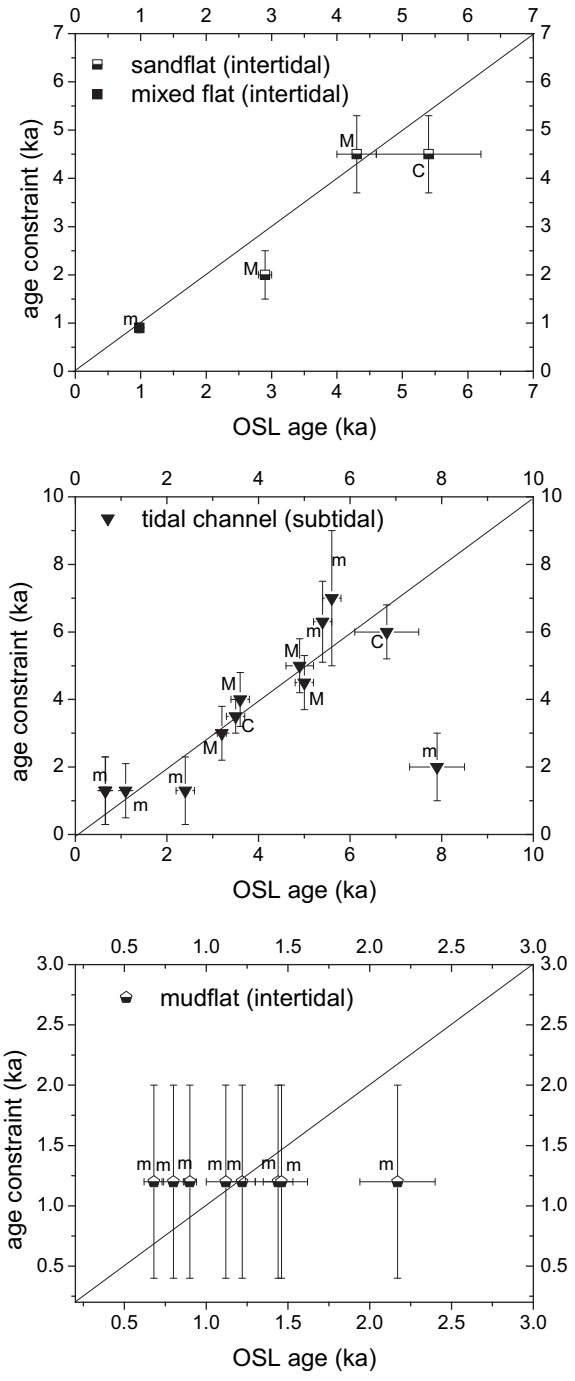

Fig. 6. Summary of the empirical study. OSL ages are plotted against their age constraint. Symbols indicate depositional environment and letters indicate D_e statistics: M = MAM-3, C = CAM, m = arithmetical mean. Details of tidal environments are listed in Table 2.

dose response curves obtained from different aliquot sizes). Amongst the samples measured with ≤6 luminescent grains per aliquot, 3 samples (LV41,43,44) show normally distributed logarithmic (ln) D_es; 3 samples (LV40,42,47) show a positively skewed ln D_e distribution and 1 sample (LV35) displays a negative ln D_e distribution (Fig. 5). From the decision protocol followed the minimum age model with 3 parameters (MAM-3, Galbraith et al., 1999) for all but one sample exhibiting positively skewed ln D_e distribution (LV40,42,47). For normally distributed ln D_e values (LV41,44) followed the central age model (CAM, Galbraith et al., 1999). For 6 samples the decision protocol led to MAM-3 (LV35,40,42,43,44,47), but significant differences between arithmetical mean D_e and MAM-3 D_e are only obtained for 2 samples (LV40,43, Table 3) as also shown by the radial plots (Fig. 5). The comparison with the age constraints shows that 10 optical ages are accurate (LV40,41, 42,43,44,45,47,345,232,233), 3 ages are overestimated (LV35,228,04), 1 age is possibly overestimated (LV227) and 10 ages are ordered correctly (i.e. stratigraphically consistent but with unknown accuracy, LV48,226,231,01,02,03,06,08,09,10). From the 10 accurate ages 8 ages are obtained from tidal channels regardless the mean high-water depth, 1 age is from sandflat and 1 age is from mixed flat (Fig. 6). From 3 overestimated ages one age is from tidal channel, one age is from sandflat and 1 age is from mudflat (Fig. 6). Both fine silt as well as fine sand quartz yields overestimated ages. Accurate ages are obtained from MAM-3, CAM and arithmetical mean, and overestimated ages are obtained from MAM-3 and arithmetical mean statistics. Dose rate data used for age estimation are listed in Table 1.

7. Discussion

The consideration of transport and depositional processes, and potential reworking of the sediment record over the long term, reveals that bleaching of the dosimeter is the major challenge of optical dating of tidal sediments. We deduce from our conceptual considerations that (i) all grains <300 mm are in suspension at some point during a tidal cycle (Fig. 2), (ii) the SSC is >0.1 g l^{-1} at 1 m water depth in most areas across tidal flats, (iii) the SSC decreases almost exponentially with vertical distance from the water–sediment interface (Fig. 2), and (iv) in very high SSC flocculation can occur and the area of maximum SSC migrates over the tidal flat. From the studies of Ditlefsen (1992) and Richardson (2001) we infer for the quartz fast component used here, that bleaching is poor where water depth is >0.5 m and where water contains >0.05 g l^{-1} SSC. Thus, it is not reasonable to assume that all grains would be sufficiently bleached during the tidal cycle. The process of reworking (i.e. re-suspension) could compensate for unfavourable bleaching conditions because the recurrence rate of the reworking trigger is monthly to seasonally in a tidal setting (e.g. Andersen et al., 2006). Moreover, exposure to sunlight during ebb tide might also contribute to sufficient bleaching. The variability of the reworking process and the SSC over a tidal flat is, however, extreme in both time and space hindering unequivocal 'bleaching rules' to be ascribed to tidal sub-environments. Also, we have to infer that a single grain does not necessarily carry the age information related to the last exposure to daylight but the age information related to the most intensive bleaching event which is not necessarily the last one. Given the time resolution of the OSL technique, this fact should have a negligible impact on the OSL age accuracy: in tidal flats with low sedimentation rate (e.g. <1 mm/a) almost all grains are exposed during ebb tide and with high sedimentation rate the dose differences are supposedly negligible.

The empirical part of our study does not fully confirm the above: out of 13 only one tidal-channel age is overestimated, out of 2 only one sandflat age and out of 9 only one mudflat age is overestimated. Thus, accurate and overestimated ages are obtained from all tidal sub-environments tested here and silt grains are not necessarily better bleached than sand grains. Amongst the statistically most meaningful samples (i.e. 2–4 luminescent grains/aliquot, Table 3) 5 samples show normal distribution of their ln D_e values and 4 samples show positively skewed distribution (Fig. 5). The latter 4 samples are from subtidal channels and from intertidal sandflats and the first 5 samples are from tidal channels, indicating that daylight exposure during ebb tide is unimportant. The decision protocol led to the correct age model for positively skewed samples

Table 4
Result of OSL analysis. Model parameter values are derived from MAM-3 and CAM statistics. Ages are labelled 'accurate', if an age constraint with a reasonable uncertainty is available. All other ages are labelled 'correct' or 'overestimated' according to stratigraphic constraints. For age constraints see Table 2 and details in Section 4.

Sample code	D_e (mean)$\pm\sigma$ (Gy)	D_e (model, Gy)	Model parameter values	OSL age (ka, $\pm1\sigma$)	Comment age
LV35	3.7 ± 0.1	2.7 ± 0.1	$P = 0.04$ $\sigma = 0.4$ $D_{emin} = 2.18$	2.9 ± 0.1	overestimated
LV40	9.6 ± 1.2	5.7 − 0.1/+0.4	$p = 0.0014$ $\sigma = 0.4$ $D_{emin} = 3.46$	5.0 ± 0.2	accurate
LV41	7.4 ± 0.5.41	7.4 ± 0.8	$\hat{\sigma} = 31$	6.8 ± 0.7	accurate
LV42	4.9 ± 0.2	4.3 ± 0.1	$p = 0.5$ $\sigma = 0.3$ $D_{emin} = 3.28$	3.6 ± 0.2	accurate
LV43	7.0 ± 0.2	5.5 − 0.2/+0.3	$p = 0.009$ $\sigma = 0.3$ $D_{emin} = 4.55$	4.9 ± 0.3	accurate
LV44	5.8 ± 0.2	5.7 ± 0.8 (CAM) 4.6 − 0.2/+0.3 (MAM-3)	$\hat{\sigma} = 367$ $p = 0.03$ $\sigma = 0.3$ $D_{emin} = 3.8$	5.4 ± 0.8 4.3 ± 0.3	accurate
LV45	3.5 ± 0.1	3.5 ± 0.2	$\hat{\sigma} = 87$	3.5 ± 0.2	accurate
LV47	4.8 ± 0.2	4.4 ± 0.1	$p = 0.7$ $\sigma = 0.3$ $D_{emin} = 3.39$	3.2 ± 0.1	accurate
LV48	8.4 ± 0.2	–	–	5.6 ± 0.2	correct
LV226	1.20 ± 0.02	–	–	0.66 ± 0.02	correct
LV227	3.3 ± 0.3	–	–	2.4 ± 0.2	possibly overestimated
LV228	4.7 ± 0.3	–	–	7.9 ± 0.6	overestimated
LV345	1.8 ± 0.05		–	0.98 ± 0.04	accurate
LV231	1.6 ± 0.02	–	–	0.65 ± 0.04	correct
LV232	1.75 ± 0.05	–	–	1.10 ± 0.05	accurate
LV233	6.5 ± 0.2	–	–	5.4 ± 0.2	accurate
LV01	2.95 ± 0.06	–	–	1.44 ± 0.09	apparently correct
LV02	3.62 ± 0.05	–	–	1.22 ± 0.08	apparently correct
LV03	3.84 ± 0.02	–	–	1.46 ± 0.16	correct
LV04	4.45 ± 0.02	–	–	2.17 ± 0.23	overestimated
LV06	2.44 ± 0.04	–	–	0.90 ± 0.04	correct
LV08	2.08 ± 0.06	–	–	0.68 ± 0.06	correct
LV09	1.80 ± 0.05	–	–	0.80 ± 0.07	correct
LV10	2.10 ± 0.04	–	–	1.12 ± 0.12	correct

(i.e. MAM) and unskewed samples (i.e. CAM) with the exception of 2 samples (LV35,43) for which skewness did not correspond to the age model. The distributions are generated by multiple-grain aliquots (estimated 2–6 luminescent grains/aliquot according to Duller, 2008) and could therefore contain artefact components which could only be identified by comparison with single-grain data (Arnold and Roberts, 2009). We do not have these data and thus, the significance of reworking processes remains a hypothesis to be proven in subsequent research.

The statistical analyses aided identifying incompletely bleached samples and the resulting statistical treatment using MAM-3 did affect 3 samples (LV35,40,43). Surprisingly, one of these samples (LV43) shows normal D_e distribution and another sample (LV35) remains overestimated. This observation confirms the hypothesis resulting from the conceptual model: incremental bleaching due to frequent reworking increases the degree of bleaching of individual grains and hence the accuracy of the optical age.

From the 3 overestimated optical ages one age can be explained: LV228 is from the base of one of the late-Holocene channels which incised deeply into mid-Holocene channels. The new channel reworked the sand of the previous channel and re-deposited it at greater depth due to its deep incision. Most quartz grains of this sample carry the dose acquired since the previous depositional event. Single-grain measurements have here the potential to improve the results. For the other overestimated ages we can only speculate on the basis of the knowledge acquired in this study: reworking was insufficient or reworking occurred alongside high SSC.

Two samples point to the shortcoming of the age constraints used in this study: LV01 and LV02 seem to return correct ages (Fig. 6) but in an age–depth model the ages appear to be overestimated (Mauz and Bungenstock, 2007). We conclude from this that assessment on accuracy is ultimately made in the course of a geological interpretation of the age data.

Two samples (LV40,41) show Th/U ratio of ~4.8 (Table 4) indicating post-mortem Uranium uptake by mollusc shells. Given the short period of uptake (<6 ka) the accuracy of the ages is likely not to be affected by the secular disequilibrium. In fact, LV40 returns an accurate age.

Two factors impair our study about the reliability of optical ages of tidal sediments: (i) unbalanced representation of tidal sub-environments by the OSL samples investigated and (ii) low OSL sensitivity of a considerable part of the quartz grains. Both factors are hard to avoid: tidal-channel deposits represent a large part of the fossil intertidal deposits (de Boer, 1998) due to their lateral migration particularly during the late Holocene when sea level stabilised and quartz with low OSL sensitivity can be encountered everywhere.

8. Conclusions

The factors controlling bleaching in tidal environments are tidal currents, SSC, waves, channel migration, plant biomass and water salinity. Thanks to the intensive study of Europe's tidal coast, many of these factors are quantified, allowing us, in principle, to infer the bleaching potential and thus, the reliability of optical ages of tidal sediments. These achievements notwithstanding unequivocal 'bleaching rules' cannot be ascribed to individual tidal sub-environments due to temporal and spatial variability of tidal transport and deposition. The empirical study indicates that tidal reworking of sediments is crucial for OSL zeroing as long as it takes place in shallow water while daylight exposure during ebb tide seems to play a minor role.

The degree of bleaching is not predictable and therefore small aliquots or ideally, single grains should be measured.

Acknowledgements

We are grateful to Edward Anthony who provided the S-cores from the French coast and Susan Packman who helped with processing the samples in the OSL laboratory. This work was supported by Synthesys grant BE-TAF-1630. The study is a contribution to the IGCP 495 project.

Appendix. Supplementary material

Supplementary information associated with this article can be found in the on-line version, at doi:10.1016/j.quageo.2010.05.004.

References

Adamiec, G., Aitken, M., 1998. Dose-rate conversion factors: update. Ancient TL 16, 37–50.
Aitken, M., 1985. Thermoluminescence Dating. Academic Press, London, 378 pp.
Andersen, T.J., Pejrub, M., Nielsen, A.A., 2006. Long-term and high-resolution measurements of bed-level changes in a temperate, microtidal coastal lagoon. Marine Geology 226, 115–125.
Andersen, T.J., Pejrup, M., 2001. Suspended sediment transport on a temperate, microtidal mudflat, the Danish Wadden Sea. Marine Geology 173, 69–85.
Arnold, L.J., Roberts, R.G., 2009. Stochastic modelling of multi-grain equivalent dose (D_e) distributions: implications for OSL dating of sediment mixtures. Quaternary Geochronology 4, 204–230.
Baeteman, C., Declercq, P.-Y., 2002. A synthesis of early and middle Holocene coastal changes in the Belgian lowlands. Belgeo 2, 77–107.
Baeteman, C., 2005. How subsoil morphology and erodibility influence the origin and pattern of late Holocene tidal channels: case studies from the Belgian coastal lowlands. Quaternary Science Reviews 24, 2146–2162.
Baeteman, C., 2008. Radiocarbon dated sediment sequences from the Belgian coastal plain: testing the hypothesis of fluctuating or smooth late Holocene relative sea-level rise. The Holocene 18 (8), 1219–1228.
Baeteman, C., Beets, D.J., van Strydonck, M., 1999. Tidal crevasse splays as the cause of rapid changes in the rate of aggradation in the Holocene tidal deposits of the Belgian Coastal Plain. Journal of Quaternary International 56, 3–13.
Baeteman, C., Scott, D.B., van Strydonck, M., 2002. Changes in coastal zone processes at a high sea-level stand: a late Holocene example from Belgium. Journal of Quaternay Science 17 (5–6), 547–559.
Bailey, R.M., Arnold, L.J., 2006. Statistical modelling of single grain quartz D_e distributions and an assessment of procedures for estimating burial dose. Quaternary Science Reviews 25, 2475–2502.
Bailiff, I.K., Tooley, M.J., 2000. Luminescence dating of fine-grain Holocene sediments from a coastal setting. In: Shennan, I., Andrews, J. (Eds.), Holocene Land–Ocean Interaction and Environmental Change Around the North Sea, vol. 166. Geol. Soc. Spec. Publ., pp. 55–67.
Berger, G.W., 1990. Effectiveness of natural zeroing of the thermoluminescence in sediments. Journal of Geophysical Research 95 (B8), 12375–12397.
de Boer, P.L., 1998. Intertidal sediments: composition and structure. In: Eisma, D. (Ed.), Intertidal Deposits: River Mouths, Tidal Flats and Coastal Lagoons. CRC Marine Science Series, pp. 345–381.
Boomer, I., Horton, B.P., 2006. Holocene relative sea-level movements along the North Norfolk coast, UK. Palaeogeography, Palaeoclimatology. Palaeoecology 230, 32–51.
Brennan, B.J., 2003. Beta doses to spherical grains. Radiation Measurements 37, 299–303.
Bungenstock, F., Schäfer, A., 2009. The Holocene relative sea-level curve for the tidal basin of the barrier island Langeoog, German Bight, southern North Sea. Global and Planetary Change 66 (1–2), 34–51.
Clarke, M.L., Rendell, H.M., 2000. The development of a methodology for luminescence dating of Holocene sediments at the land–ocean interface. In: Shennan, I., Andrews, J. (Eds.), Holocene Land–Ocean Interaction and Environmental Change Around the North Sea, vol. 166. Geol. Soc. Spec. Publ., pp. 69–86.
Denys, L., Baeteman, C., 1995. Holocene evolution of relative sea level and local mean high water spring tides in Belgium – a first assessment. Marine Geology 124, 1–19.
Ditlefsen, C., 1992. Bleaching of K-feldspars in turbid water suspensions: a comparison of photo and thermoluminescence signals. Quaternary Science Reviews 11, 33–38.
Duller, G.A.T., 2003. Distinguishing quartz and feldspar in single grain luminescence measurements. Radiation Measurements 37, 161–165.
Duller, G.A.T., 2008. Single-grain optical dating of Quaternary sediments: why aliquot size matters in luminescence dating. Boreas 37, 589–612.
Galbraith, R.F., Roberts, R.G., Laslett, G.M., Yoshida, H., Olley, J.M., 1999. Optical dating of single and multiple grains of quartz from Jinmium rock shelter, northern Australia. Part I experimental design and statistical models. Archaeometry 41, 339–364.
Hjulstrøm, F., 1935. Studies in the morphological activities of rivers as illustrated by the River Fyris. Bulletin of the Geological Institutions of the University of Uppsala 25, 221–528.
Hong, D.-G., Choi, M.S., Han, J.-H., Cheong, C.-S., 2003. Determination of sedimentation rate of a recently deposited tidal flat, western coast of Korea, using IRSL dating. Quaternary Science Reviews 22, 1185–1189.
Jacobs, Z., 2008. Luminescence chronologies for coastal and marine sediments. Boreas 37, 508–535.
Lian, O.B., Hu, J., Huntley, D.J., Hicock, S.R., 1995. Optical dating studies of Quaternary organic-rich sediments from south-western British Columbia and northwestern Washington State. Canadian Journal of Earth Sciences 32, 1194–1207.
Madsen, A.T., Murray, A.S., Andersn, T.J., Pejrup, M., 2007a. Temporal changes of accretion rates on an estuarine salt mash during the late Holocene – reflection of local sea level changes? The Waddden Sea, Denmark. Marine Geology 242, 221–233.
Madsen, A.T., Murray, A.S., Andersn, T.J., Pejrup, M., 2007b. Optical dating of young tidal sediments in the Danish Wadden Sea. Quaternary Geochronology 2, 89–94.
Madsen, A.T., Murray, A.S., Andersen, T.J., Pejrup, M., Breuning-Madsen, H., 2005. Optically stimulated luminescence dating of young estuarine sediments: a comparison with ^{210}Pb and ^{137}Cs dating. Marine Geology 214, 251–268.
Mauz, B., Bungenstock, F., 2007. How to reconstruct trends of late Holocene relative sea level: a new approach using tidal flat clastic sediments and optical dating. Marine Geology 237, 225–237.
Mauz, B., Bode, T., Mainz, E., Blanchard, H., Hilger, W., Dikau, R., Zöller, L., 2002. The luminescence dating laboratory at the University of Bonn: equipment and procedures. Ancient TL 20, 53–61.
Mauz, B., Packman, S., Lang, A., 2006. The alpha efficiency of silt-sized quartz: new data obtained by single and multiple aliquot protocols. Ancient TL 24, 47–52.
Merckelbach, L.M., Ridderinkhof, H., 2006. Estimating suspended sediment concentration using backscatterance from an acoustic Doppler profiling current meter at a site with strong tidal currents. Ocean Dynamics 56, 153–168.
Miller, M.C., McCave, I.N., Komar, P.D., 1977. Threshold of sediment motion under unidirectional currents. Sedimentology 24, 507–527.
Mrani Alaoui, M., 2006. Evolution des environments sedimentaires Holocenes de la plaine maritime Flamande du nord de la France: Eustatisme et processus. Unpublished PhD Thesis, Université du Littoral, Dunkerque, 165 pp.
Murray, A.S., Wintle, A.G., 2000. Luminescence dating of quartz using an improved single-aliquot regenerative-dose protocol. Radiation Measurements 32, 57–73.
Nielsen, P., 1984. Field measurements of time-averaged suspended sediment concentrations under waves. Coastal Engineering 8, 51–72.
Olley, J.M., Caitcheon, G., Murray, A., 1998. The distribution of apparent dose as determined by optically stimulated luminescence in small aliquots of fluvial

quartz: implications for dating young sediments. Quaternary Geochronology 17, 1033–1040.
Pejrub, M., 1986. Parameters affecting fine-grained suspended sediment concentration in a shallow micro-tidal estuary, Ho Buget, Denmark. Estuarine, Coastal and Shelf Science 22, 241–254.
Plater, A.J., Poolton, N.R.J., 1992. Interpretation of Holocene sea level tendency and intertidal sedimentation in the Tees estuary using sediment luminescence techniques: a variability study. Sedimentology 39, 1–15.
Prescott, J.R., Hutton, J.T., 1994. Cosmic ray contribution to dose rates for luminescence and ESR dating: large depths and long-term time variations. Radiation Measurements 23, 497–500.
Reineck, H.E., 1958. Longitudinale Schraegschichten im Watt. Geologische Rundschau 37, 73–82.
Richardson, C.A., 2001. Residual luminescence signals in modern coastal sediments. Quaternary Science Reviews 20, 887–892.
Roberts, H.M., Plater, A.J., 2005. Optically Stimulated Luminescence (OSL) Dating of Sands Underlying the Gravel Beach Ridges of Dungeness and Camber, Southeast England, UK, vol. 27. Centre for Archaeology Report, p. 83.
Roberts, H.M., Plater, A.J., 2007. Reconstruction of Holocene foreland progradation using optically stimulated luminescence (OSL) dating: an example from Dungerness, UK. The Holocene 17, 495–505.
Rodnight, H., 2008. How many equivalent dose values are needed to obtain a reproducible distribution? Ancient TL 26, 3–9.
Sanderson, D.C.W., Bishop, P., Stark, M., Alexander, S., Penny, D., 2007. Luminescence dating of canal sediments from Angkor Borei, Mekong delta, Southern Cambodia. Quaternary Geochronology 2, 322–329.
Streif, H., 2004. Sedimentary record of Pleistocene and Holocene marine inundations along the North Sea coast of Lower Saxony, Germany. Quaternary International 112, 3–28.
van der Spek, A.J.F., Beets, D.J., 1992. Mid-Holocene evolution of a tidal basin in the western Netherlands: a model for future changes in the northern Netherlands under conditions of accelerated sea-level rise? Sedimentary Geology 80, 185–197.
Van Lengen, H., 1978. Historisch-Landeskundliche Exkursionskarte von Niedersachsen — Maβstab 1:50000, Blatt Esens. Erläuterungsheft, Hildesheim. 179.